Main Manuscript for

The July 2026 North American wildfire smoke event was three times deadlier due to climate change

Dmitri A. Kalashnikov[1‡], Emily L. Williams[1‡], John T. Abatzoglou[2], Cong Yin[1], Wenli Ni[3], Nicholas J. Nassikas[3,4], Matthew W. Jones[5]

[1] Earth Institute, University of California, Merced, Merced, CA, 95343, USA
[2] Management of Complex Systems Department, University of California, Merced, Merced, CA, 95343, USA
[3] Center for Climate, Health and the Global Environment, Harvard T.H. Chan School of Public Health, Boston, Massachusetts, USA
[4] Division of Pulmonary, Critical Care, and Sleep Medicine, Beth Israel Deaconess Medical Center, Boston, Massachusetts, USA
[5] Tyndall Centre for Climate Change Research, School of Environmental Science, University of East Anglia, Norwich, UK

‡ authors contributed equally

* Corresponding authors: Dmitri A. Kalashnikov and Emily L. Williams
Email: dkalashnikov@ucmerced.edu; emilywilliams@ucmerced.edu

Author Contributions: DAK, ELW, JTA, and CY developed the methodology, curated datasets, and conducted the analysis. DAK, ELW, JTA, and CY wrote the initial manuscript draft, and all authors contributed to text revisions.

Competing Interest Statement: The authors declare no competing interests.

Classification: Physical Sciences; Earth, Atmospheric, and Planetary Sciences

Keywords: wildfire smoke, attribution, climate change, mortality

This file includes:

Main Text
Figures 1 to 2

Abstract

In mid-July 2026, numerous fast-burning wildfires affected western Ontario and northern Minnesota, resulting in extensive smoke across eastern North America. Here, we conduct a rapid attribution analysis of the 14–21 July smoke event, quantifying the change in wildfire smoke (WFS) $PM_{2.5}$ concentrations and mortality compared to a counterfactual world without anthropogenic climate change (ACC). We find that ACC increased WFS $PM_{2.5}$ concentrations by approximately three-fold. As a result, population exposure to regulatory exceedances of WFS $PM_{2.5}$ concentrations (>35 $\mu g/m^3$) amounted to 268 million person-days, of which 157 million are attributable to ACC. We estimate 770 excess deaths attributable to observed WFS $PM_{2.5}$ exposure, a three-fold increase compared to the counterfactual scenario. This rapid impact-attribution assessment of WFS $PM_{2.5}$-related mortality provides a methodological framework for quantifying the ACC contribution to other acute air pollution episodes globally.

Main Text

Introduction

In mid-July 2026, widespread wildfires burned in western Ontario and northern Minnesota, resulting in extensive wildfire smoke (WFS) and unhealthy levels of fine particulate matter ($PM_{2.5}$) air pollution across eastern North America (ENA) (1). This event was reminiscent of the extreme 2023 Canadian wildfire season, when unprecedented fire activity produced widespread smoke impacts across densely populated regions of ENA (2–4). The recurrence of extreme smoke episodes, combined with demonstrated linkages between anthropogenic climate change (ACC) and wildfire activity (3), has raised urgent questions about future trajectories of air quality in this region and the associated health impacts.

Acute exposure to WFS is associated with a wide range of health impacts, including cardiopulmonary diseases and premature mortality (5, 6). These impacts can occur far from the fires due to long-range smoke transport (7, 8). Despite growing adoption of attribution methods in climate science, including prior studies that quantify the ACC contribution to WFS and mortality (9), to our knowledge no prior studies have quantified the contribution of ACC to WFS-associated mortality tied to specific wildfire events. Here, we quantify the extent to which ACC amplified WFS population exposure and associated mortality over ENA in mid-July 2026.

Methods

We conduct our attribution analysis over the region of ENA most impacted by WFS during the July 2026 event (36°–52°N, 100°–60°W). For burned area (BA), we analyze 13–16 July which represents the main burning period, while smoke accumulation and transport in the atmosphere occurred over the following week. We therefore analyze 14–21 July for WFS exposure and mortality. We first model 2026 BA over western Ontario and northern Minnesota, where the vast majority of BA occurred during the event (Fig. 1A), by constructing an ensemble of 11 univariate linear regression models that use five variables at different temporal lags from the ERA5-Land reanalysis (10) as predictors. These variables are vapor pressure deficit (VPD), Fire Weather Index (FWI), Fine Fuel

Moisture Code (FFMC), Duff Moisture Code (DMC), and Drought Code (DC). We then estimate what the preindustrial, or "counterfactual," BA would have been by removing the ACC influence on the predictors using a suite of 12 climate models from the Coupled Model Intercomparison Project Phase 6 (CMIP6) (11), that each had at least three ensemble members, and rerunning the regression models with the counterfactual predictor estimates. From these, we obtain a scaling factor for WFS $PM_{2.5}$ by dividing actual modeled BA by the counterfactual BA. Next, we retrieve analysis fields of near-surface WFS $PM_{2.5}$ concentrations from the High-Resolution Rapid Refresh smoke model (HRRR-Smoke) at 3-km resolution (12), and adjust these concentrations downward for the counterfactual scenario using the scaling factor. Finally, we estimate excess mortality attributable to actual and counterfactual WFS $PM_{2.5}$. This is done by feeding actual and counterfactual WFS $PM_{2.5}$ into a concentration-response function (CRF) designed for modeling excess mortality associated with $PM_{2.5}$ exposure. For the counterfactual, we report exposure and mortality derived from the CMIP6 multi-model mean (MMM) and the interquartile range (IQR) across the modeled counterfactual estimates. (See SI Appendix, Supplemental Methods for details).

Results

During 13–16 July, wildfires burned 3642 km^2 of mostly boreal forest in western Ontario and northern Minnesota, representing the largest 4-day BA over this region in the 2001–2026 period and larger than all but three previous annual totals (Fig. 1A–B). Counterfactual modeling reveals that BA would have been lower by a factor of 2.86 (IQR: 1.38–4.97) without the influence of ACC (Fig. 1C). Assuming linear scaling between BA and WFS $PM_{2.5}$, we estimate that ACC increased WFS $PM_{2.5}$ concentrations by this factor during the smoke event. Severe and widespread air quality impacts occurred across ENA during the following week, peaking on 16–18 July (Fig. 1D–F). These concentrations of WFS $PM_{2.5}$ exceeded United States federal air quality regulatory standards (>35 $\mu g/m^3$, hereafter 'exceedances') across >1 million km^2 on each of these days. However, extents would have been substantially smaller in a counterfactual world, with a 76% reduction on 18 July (Fig. 1F,I).

During 14–21 July, exposure to WFS $PM_{2.5}$ exceedances totaled 267.85 million person-days compared to 111.12 million (IQR: 39.23–223.19 million) in the counterfactual, equating to 157 million (IQR: 45–229 million) additional person-days directly attributable to ACC (Fig. 2A–B). We estimate that exposure to observed WFS $PM_{2.5}$ across all concentrations resulted in 770 excess deaths during 14–21 July compared to 276 excess deaths (IQR: 160–564) in the counterfactual, a nearly three-fold increase (Fig. 2D–E). However, these results are highly sensitive to the choice of CRF used (13), with mean estimates of 393–1410 excess deaths in the actual scenario and 139–516 excess deaths for the counterfactual, depending on the CRF. Among states and provinces, New York experienced the greatest smoke impacts from this event, with 55 million person-days of exposure to WFS $PM_{2.5}$ exceedances and an estimated 153 attributable excess deaths, which would have been 46% and 64% lower, respectively, absent ACC (Fig. 2C,F).

Discussion

In mid-July 2026, widespread WFS from western Ontario and northern Minnesota impacted densely populated regions of ENA. We estimate that ACC approximately

tripled BA and WFS $PM_{2.5}$ concentrations, leading to 157 million (IQR: 45–229 million) additional person-days of exposure to WFS $PM_{2.5}$ exceedances and 494 (IQR: 206–610) additional excess deaths. The threefold increase in BA and WFS $PM_{2.5}$ that we attribute to ACC, compared to the counterfactual, is consistent with both the expected response in flammability-limited fire regimes in boreal forests and ACC influence on fuel aridity metrics (14). For example, earlier spring snowmelt lengthens the seasonal drying period while hotter temperatures promote increases in atmospheric and fuel aridity that can directly increase BA and associated smoke impacts in populated regions (2).

We note several caveats to our rapid attribution analysis. *First*, we use modeled WFS $PM_{2.5}$ from HRRR-Smoke rather than direct observations due to its near-real time availability on a regular grid that facilitates this type of analysis; this product has additionally shown good performance at simulating previous high-impact smoke events (12). *Second*, we scale WFS $PM_{2.5}$ by the ACC-attributable change in BA rather than directly simulating smoke emissions, chemistry, and transport in the counterfactual scenario. This smoke event resulted from a combination of extreme heat, winds, and dry fuels that drove record-breaking BA in western Ontario and northern Minnesota that were followed by a large-scale atmospheric flow configuration conducive for smoke transport into densely populated urban centers; potential ACC-driven changes to such large-scale atmospheric dynamics are not explored herein. *Finally*, we use simple but reproducible linear models of annual BA that capture a range of fuel aridity metrics and temporal lags, but may not capture more complex processes tied to fuels, ignition, and fire behavior. Nevertheless, our results suggest that ACC substantially contributed to the extreme fire extent underpinning the July 2026 smoke event over ENA and the resulting public health burden.

The extension of rapid attribution analyses to direct human impacts is an emerging area of focus for attribution science (15). By propagating the influence of ACC from BA and WFS $PM_{2.5}$ concentrations directly to population exposure and mortality associated with the July 2026 smoke event using near-real time data, we provide an event-specific estimate of the health burden attributable to ACC for this extreme event. Applying this approach after other high-impact smoke events can help place their immediate public health consequences in the context of a changing climate and could inform policy discussions to mitigate adverse outcomes in the future. More broadly, this framework could be adapted to other extreme events that have quantifiable linkages to direct and indirect human health impacts.

Data and Software Availability

Data and code have been deposited to Zenodo (DOI: 10.5281/zenodo.23318569) (16).

Acknowledgments

The authors have no external funding to report.

References

1. National Oceanic and Atmospheric Administration, NOAA satellites played critical role in monitoring historic smoke event (2026). Available at

https://www.nesdis.noaa.gov/news/noaa-satellites-played-critical-role-monitoring-historic-smoke-event. [Accessed 7 October 2026].

2. P. Jain, *et al.*, Drivers and impacts of the record-breaking 2023 wildfire season in Canada. *Nat. Commun.* **15**, 6764 (2024).

3. M. C. Kirchmeier-Young, *et al.*, Human driven climate change increased the likelihood of the 2023 record area burned in Canada. *Npj Clim. Atmos. Sci.* **7**, 316 (2024).

4. M. W. Jones, *et al.*, State of wildfires 2023–2024. *Earth Syst. Sci. Data* **16**, 3601–3685 (2024).

5. J. T. Pryor, L. O. Cowley, S. E. Simonds, The physiological effects of air pollution: Particulate matter, physiology and disease. *Front. Public Health* **10**, 882569 (2022).

6. G. Chen, *et al.*, Wildfire smoke and health: current evidence, mechanisms, and future challenges. *Lancet* **408**, 1129–1142 (2026).

7. Q. Zhang, *et al.*, Long-range $PM_{2.5}$ pollution and health impacts from the 2023 Canadian wildfires. *Nature* **645**, 672–678 (2025).

8. Z. Wang, *et al.*, Severe global environmental issues caused by Canada's record-breaking wildfires in 2023. *Adv. Atmos. Sci.* **41**, 565–571 (2024).

9. B. E. Law, *et al.*, Anthropogenic climate change contributes to wildfire particulate matter and related mortality in the United States. *Commun. Earth Environ.* **6**, 336 (2025).

10. J. Muñoz-Sabater, *et al.*, ERA5-Land: a state-of-the-art global reanalysis dataset for land applications. *Earth Syst. Sci. Data* **13**, 4349–4383 (2021).

11. V. Eyring *et al.*, Overview of the Coupled Model Intercomparison Project Phase 6 (CMIP6) experimental design and organization. *Geosci. Model Dev.* **9**, 1937–1958 (2016).

12. F. K. Chow, *et al.*, High-resolution smoke forecasting for the 2018 Camp Fire in California. *Bull. Am. Meteorol. Soc.* **103**, E1531–E1552 (2022).

13. G. Chen, *et al.*, Mortality risk attributable to wildfire-related $PM_{2.5}$ pollution: a global time series study in 749 locations. *Lancet Planet. Health* **5**, e579–e587 (2021).

14. P. Jain, D. Castellanos-Acuna, S. C. P. Coogan, J. T. Abatzoglou, M. D. Flannigan, Observed increases in extreme fire weather driven by atmospheric humidity and temperature. *Nat. Clim. Chang.* **12**, 63–70 (2022).

15. S. Undorf, *et al.*, Approaches, challenges and applications of climate change impact attribution. *Nat. Rev. Earth Environ.* **7**, 469–488 (2026).

16. D. A. Kalashnikov, *et al.*, Data and code accompanying: “The July 2026 North American wildfire smoke event was three times deadlier due to climate change.” Zenodo. https://doi.org/10.5281/zenodo.23318569. Deposited 12 October 2026.

Figures

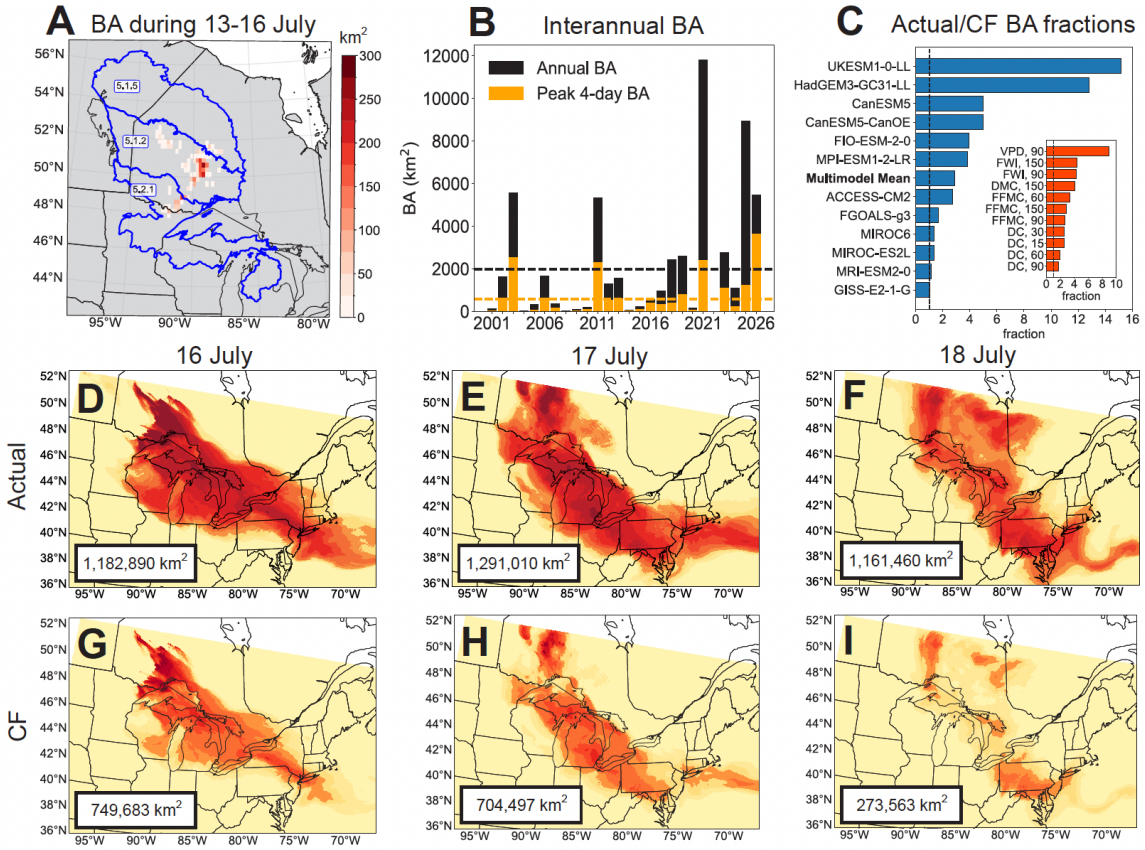


Fig. 1. Actual and counterfactual (CF) BA and $PM_{2.5}$. (A) Total estimated BA from MODIS during 13–16 July, 2026, in the three ecoregions (blue polygons) considered in this analysis. (B) Total annual and peak 4-day BA during 2001–2026 over this domain. Dashed lines show corresponding 2001–2025 means. (C) Median fractions ("scaling factors") of actual to counterfactual (CF) BA from an ensemble of 12 CMIP6 models and the multi-model mean. Each CMIP6 model's fraction is derived from an ensemble of 11 univariate BA models utilizing maximum time-averaged VPD, FWI, DMC, FFMC, and DC over the year trained over 2002–2024 (inset panel; fractions represent median value across the CMIP6 models for each variable). Numbers next to variable names represent the time-averaged length in days (See SI Appendix, Supplemental Methods). (D–F) Actual modeled WFS $PM_{2.5}$ concentrations during 16–18 July, 2026. Inset text shows continental areas exposed to >35 μg/m^3 of WFS $PM_{2.5}$. (G–I) As in (D–F), but for the CF scenario.

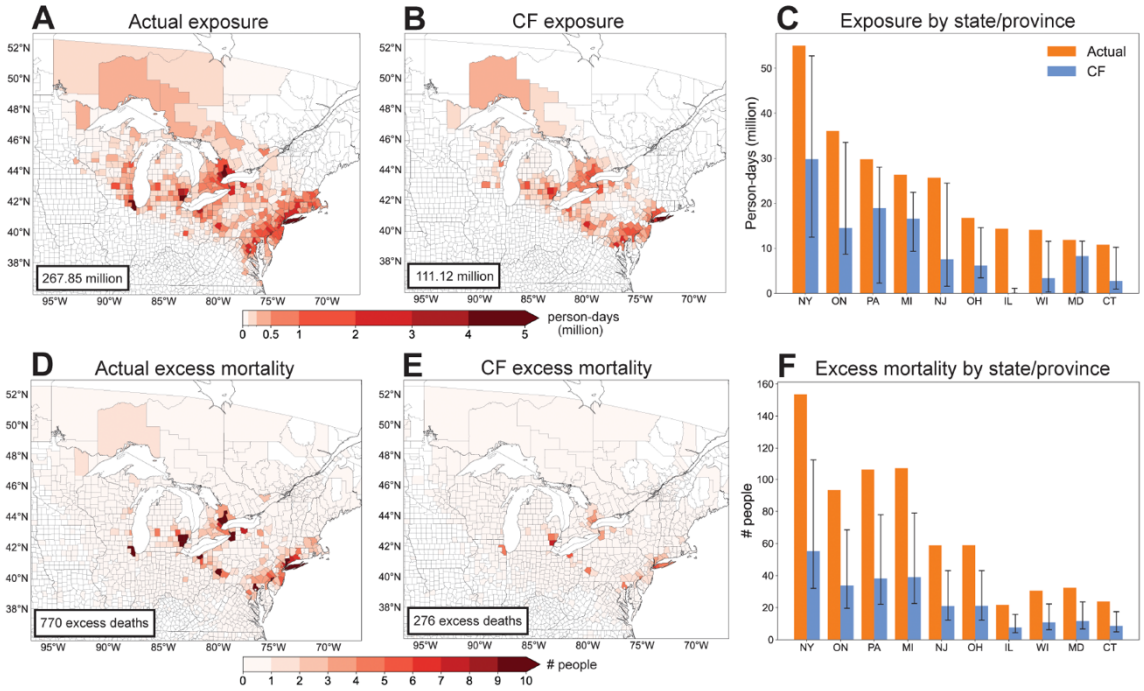


Fig. 2. Exposure to and excess mortality from WFS $PM_{2.5}$. (A–B) Total exposure (in million person-days) to WFS $PM_{2.5}$ >35 μg/m^3 during 14–21 July, 2026, at the level of counties (US) and census divisions (Canada) in (A) actual and (B) CF scenarios. White colors represent zero exposure. Inset text boxes show total exposure in person-days. (C) As in (A–B), but showing the top-10 largest states/provinces ranked by actual exposure. Error bars show the IQR of CF exposure estimated from the CMIP6 model ensemble. (D–F) As in (A–C), but for excess mortality attributable to WFS $PM_{2.5}$.

Supporting Information for

The July 2026 North American wildfire smoke event was three times deadlier due to climate change

Dmitri A. Kalashnikov[1‡], Emily L. Williams[1‡], John T. Abatzoglou[2], Cong Yin[1], Wenli Ni[3], Nicholas J. Nassikas[3,4], Matthew W. Jones[5]

[1] Earth Institute, University of California, Merced, Merced, CA, 95343, USA

[2] Management of Complex Systems Department, University of California, Merced, Merced, CA, 95343, USA

[3] Center for Climate, Health and the Global Environment, Harvard T.H. Chan School of Public Health, Boston, Massachusetts, USA

[4] Division of Pulmonary, Critical Care, and Sleep Medicine, Beth Israel Deaconess Medical Center, Boston, Massachusetts, USA

[5] Tyndall Centre for Climate Change Research, School of Environmental Science, University of East Anglia, Norwich, UK

‡ authors contributed equally

* Corresponding authors: Dmitri A. Kalashnikov and Emily L. Williams

Email: dkalashnikov@ucmerced.edu; emilywilliams@ucmerced.edu

This PDF file includes:

Supplemental Methods

Supplemental References

Supplemental Methods

Actual versus counterfactual BA and WFS $PM_{2.5}$

We develop an ensemble of empirical annual climate-BA models for the combined region encompassing three Environmental Protection Agency (EPA) North American Level III ecoregions (1) that accounted for nearly the entirety of the fire emissions of the event (regions 5.1.2, 5.1.5, and 5.2.1; Fig. 1A). Satellite-derived BA data are sourced from the Moderate Resolution Imaging Spectroradiometer (MODIS) during 2001–2026 (2), while meteorological data are retrieved from ERA5-Land. We derive five variables from ERA5-Land: VPD and four variables from the Canadian Forest Fire Danger Rating System (CFFDRS) (3) – FWI, FFMC, DMC, and DC. MODIS BA data are used to display the time series of annual and peak 4-day BA over the three combined ecoregions (2001–2026; Fig. 1B) and for the climate-BA modeling (2002–2024, described below).

Following (4), we consider 30 univariate climate-BA models from the combinations of these five variables and six different timescales (maximum 7-, 15-, 30-, 60-, 90-, and 150-day rolling averages) during 2002–2024 (Eq. 1):

$$\log(BA_i) = \alpha + \beta X + \varepsilon \quad (1)$$

Where BA_i is the BA in year i, X is the predictor variable, and ε is the error term. These models are chosen over more complex models for parsimony and because multivariate models added little explanatory power. While prior studies have used a single climate-BA model in similar efforts (5), our use of an ensemble of climate-BA models can capture uncertainties stemming from the choice of predictor variable used. Consistent with the flammability-limited fire regimes of the region, the models relate measures of fuel dryness and fire weather to annual BA. The models also include an error term (ε) to account for residual information not present in its predictor variable (e.g., quantity and location of lightning ignitions, fuel abundance, suppression efforts) that shape observed BA variability. We approximate variables for 2026 (e.g., 90-day maximum FWI) by using corrected year-to-date data through 31 August, 2026. The correction is performed by linearly regressing year-to-date (through 31 August) and annual values during 2002–2024, and adjusting 2026 data to its expected annual values based on these linear relationships.

From the 30 different climate-BA model combinations considered, we retain models based on two criteria: (i) capture at least 40% of the interannual variability in BA in the region during the 2002–2024 training period ($R^2 \geq 0.4$), and (ii) modeled interquartile range (formed by resampling ε from the historical residual errors $n = 23$ times) for 2026 includes the estimated observed BA from MODIS. A total of 11 of the 30 possible climate-BA models met these criteria (see Fig. 1C inset).

Next, we calculate counterfactual estimates of the variables used for modeling 2026 BA using a low-pass filter approach (5). First, output is retrieved from 12 different climate

models participating in CMIP6 that had at least three ensemble members for both historical (1850–2014) and SSP2-4.5 (2015–2100) experiments for the requisite variables for computing CFDDRS metrics and VPD. For each of the 12 models, model means are calculated across the ensemble members to isolate anthropogenic forcing from internal variability. Next, anomalies relative to a quasi-preindustrial climate (1850–1900) are calculated based on these 12 model means, and a 50-year low pass Butterworth filter is applied to these anomalies for each model, variable, month, and location. This further minimizes internal variability (on <50 year timespans) from ensemble mean results (6). Lastly, we calculate a multi-model mean (MMM) of the ACC response by averaging anomalies across the models. These 13 estimates (12 models and 1 MMM estimate) are bilinearly interpolated to the same resolution as the ERA5-Land data, and used to adjust ERA5-Land data on daily time scales to create counterfactual meteorological data. From these counterfactual meteorological values, counterfactual VPD and CFFDRS metrics are derived and used as input to the climate-BA models (eq. 1).

We calculate a scaling factor based on the ratio of modeled actual BA (using ERA5-Land data for 2026) to counterfactual BA (using counterfactual climate for 2026) for each combination of i) climate-BA model and ii) CMIP6 model's counterfactual climate. Differences across both climate-BA models and counterfactual estimates from the CMIP6 model suite provide a means to identify uncertainty in the resultant ACC BA signal (e.g., VPD metrics show much higher scaling factors than those from CFFDRS metrics). For each of the 12 CMIP6 models, we compute the actual to counterfactual BA fraction from each of the 11 climate-BA models and then calculate their median fraction, which ranges from 1.05–15.17 across the CMIP6 models (Fig. 1C). The MMM fraction is calculated similarly but using the MMM estimates across the 11 climate-BA models and serves as the central estimate of our scaling factor (2.86) for the WFS and mortality analyses. To quantify uncertainty, we use the IQR of the scaling factor from the CMIP6 model suite (1.38–4.97).

Next, we retrieve hourly analysis fields of near-surface WFS $PM_{2.5}$ from HRRR-Smoke during July 2026, and divide these concentrations by the three scaling factors representing the 25th percentile, mean, and 75th percentile of the CMIP6 model suite (1.38, 2.86, and 4.97). This approach preserves the spatial structure of observational $PM_{2.5}$ concentrations but modifies concentrations downward. We note that this approach assumes a linear scaling of $PM_{2.5}$ with BA, which is likely conservative as fuel consumption and fire emissions per unit BA generally increase with fuel aridity (7).

To validate our approach, we repeat the climate-BA modeling analysis using fire $PM_{2.5}$ emissions from the 5th version of the Global Fire Emissions Database (GFED5) for 2002–2022 (8) and the near-real-time (NRT) extension to GFED5 (GFED5NRT) for 2023–2026 (9). Results are similar with largely the same univariate models retained as in the climate-BA modeling (not shown). Similarly, the MMM scaling factor for actual to counterfactual $PM_{2.5}$ emissions is 2.57 (IQR: 1.30–3.49), comparable to the 2.86 (IQR: 1.38–4.97) scaling factor derived from BA. We retain the climate-BA modeling results and associated actual to counterfactual scaling factors in our analysis due to the more consistent historical availability of BA data.

Actual versus counterfactual exposure and excess mortality

Finally, we estimate exposure and excess mortality associated with the July 2026 smoke event. We select the 14–21 July period as this captures the full temporal extent of widespread WFS exposure.

For descriptive purposes, we quantify exposure to WFS in person-days for smoke-specific $PM_{2.5}$ concentrations >35 $\mu g/m^3$, which represents the EPA regulatory standard in the US. Given that these concentrations represent only the WFS component, actual $PM_{2.5}$ concentrations were higher when factoring in background pollution sources.

The excess mortality analysis uses an R programming language-based version of BenMAP, a publicly-available software used by the EPA that calculates health outcomes due to air pollution exposure (10), and is conducted at the county-level for the US and for census divisions in Canada. Baseline population and mortality data are retrieved from BenMAP for the US, then the baseline mortality incidence is divided by population for each county to estimate a mortality rate ($person^{-1}$ $year^{-1}$), and averages of these rates are calculated for each county across 2006–2020. For Canada, the baseline mortality rate (per 1000 people) is retrieved from Statistics Canada (11) for 2020–2024 for each province from which average rates are derived. Unlike for US data, here we use a temporally static population data layer for 2016 at 10-km resolution (12). This population data layer is intersected with the census division shapefile to compute total population and average mortality rate per census division. We focus on acute mortality for this rapid attribution analysis while acknowledging the potentially much larger chronic mortality associated with large-scale WFS events, as demonstrated during the 2023 Canadian wildfire season (13); a substantial chronic mortality burden may similarly result from this event.

Next, for each administrative unit, we derive the spatial and temporal 3-day (lag 0–2) average $PM_{2.5}$. To calculate excess daily mortality from short-term WFS $PM_{2.5}$ exposure, we use concentration-response functions for all-cause mortality associated with a 10 $\mu g/m^3$ increase in short-term exposure to WFS $PM_{2.5}$ (14). Note that unlike the exposure analysis, here we use all days regardless of WFS $PM_{2.5}$ concentration (i.e., we do not use the >35 $\mu g/m^3$ threshold). To capture uncertainty in the choice of risk ratio (RR) associated with each CRF, we select three different RR values from Chen et al. (14) – US-specific (1.010), North America (1.005), and global (1.019). The global values originate from the observed global response of mortality to exposure while in reality this would be expected to vary from country to country; thus this would likely lead to an overestimate of excess mortality when applied to North America. We elect to use the mean RR but not the 95% confidence interval spread, instead allowing uncertainty in excess mortality in our analysis to stem from the CMIP6 model spread.

We apply the RR to the actual and counterfactual WFS $PM_{2.5}$ data to estimate excess mortality from exposure (eq. 2–3):

$$\beta = \frac{\log(RR)}{inc} \quad (2)$$

$$\Delta Y = \left(1 - e^{-\beta \cdot \Delta x}\right) * Y_0 * Pop \quad (3)$$

Where *inc* is the incremental increase in the exposure variable (here, 10 μg/m^3), Δx is the change in acute exposure (total WFS $PM_{2.5}$ for each day for this application), *pop* is the population, Y_o is the baseline all-cause mortality rate, and ΔY is the number of attributable excess mortality cases.

Supplemental References

1. J. M. Omernik, G. E. Griffith, Ecoregions of the conterminous United States: evolution of a hierarchical spatial framework. *Environ. Manage.* **54**, 1249–1266 (2014).

2. L. Giglio, L. Boschetti, D. P. Roy, M. L. Humber, C. O. Justice, The Collection 6 MODIS burned area mapping algorithm and product. *Remote Sens. Environ.* **217**, 72–85 (2018).

3. C. E. van Wagner, *Development and structure of the Canadian Forest Fire Weather Index System* (Canadian Forestry Service, Ottawa, Canada, Forestry Technical Report 35, 1987).

4. M. C. Kirchmeier-Young, *et al.*, Human driven climate change increased the likelihood of the 2023 record area burned in Canada. *Npj Clim. Atmos. Sci.* **7**, 316 (2024).

5. B. E. Law, *et al.*, Anthropogenic climate change contributes to wildfire particulate matter and related mortality in the United States. *Commun. Earth Environ.* **6**, 336 (2025).

6. J. T. Abatzoglou, A. P. Williams, Impact of anthropogenic climate change on wildfire across western US forests. *Proc. Natl. Acad. Sci. U. S. A.* **113**, 11770–11775 (2016).

7. N. H. F. French, *et al.*, Model comparisons for estimating carbon emissions from North American wildland fire. *J. Geophys. Res.* **116** (2011).

8. G. R. van der Werf, *et al.*, Landscape fire emissions from the 5th version of the Global Fire Emissions Database (GFED5). *Sci. Data* **12**, 1870 (2025).

9. Y. Chen, *et al.*, Tracking recent extremes and interannual variability of global fire emissions using a near-real-time extension to the Global Fire Emissions Database. *Earth System Science Data Discussions* (2026).

10. J. D. Sacks, *et al.*, The Environmental Benefits Mapping and Analysis Program - Community Edition (BenMAP-CE): A tool to estimate the health and economic benefits of reducing air pollution. *Environ. Model. Softw.* **104**, 118–129 (2018).

11. Statistics Canada, Mortality rates, by age group. Table 13-10-0710-01 (2026). Available at https://doi.org/10.25318/1310071001-eng [Accessed 8 October 2026].

12. Agriculture and Agri-Food Canada, Population of Canada, 10km Gridded (2026). Available at https://open.canada.ca/data/en/dataset/c6c48391-fd2f-4d8a-93c8-eb74f58a859b [Accessed 8 October 2026].

13. Q. Zhang, *et al.*, Long-range $PM_{2.5}$ pollution and health impacts from the 2023 Canadian wildfires. *Nature* **645**, 672–678 (2025).

14. G. Chen, *et al.*, Mortality risk attributable to wildfire-related $PM_{2.5}$ pollution: a global time series study in 749 locations. *Lancet Planet. Health* **5**, e579–e587 (2021).